Electrical Engineering (2021) 103:2537–2545
https://doi.org/10.1007/s00202-021-01234-4

ORIGINAL PAPER

Research on distributed networked unbalanced harmonic control combined with APF

Xusheng Yang[1] · Xufeng Liu[2] · Wei Chen[3] · ErChao Li[3]

Received: 10 September 2020 / Accepted: 3 February 2021 / Published online: 6 March 2021

Abstract
In order to solve the unbalanced harmonics problem of multi-source and multi-inverter system, a networked hierarchical control approach is proposed, based on the structure of hierarchical control and combined with active parallel filters (APF). In the control approach, the distributed generator (DG) consists of primary and secondary control. In the primary controller and the secondary controller, some basic controls are proposed and modified, which maintain the stable operation of the system. Similarly, a DG compensation and APF-coordinated compensation controller are designed, which coordinate with each other to control the power quality of the system. When the DG compensator cannot fully compensate the sensitive load bus (SLB) by itself, the APF controller can calculate compensation through coordinated control management, then using the APF auxiliary compensator for compensation. Not only does the proposed approach compensate the voltage unbalanced harmonic at SLB, but it also improves the precision of power distribution and load current sharing. Finally, simulation results can validate the effectiveness and feasibility of the proposed approach.

Keywords Microgrids (mgs) · Distributed generator · Sensitive load bus · Voltage unbalance compensation · Harmonic compensation · Active parallel filters

1 Introduction

In order to solve the accessing problem of distributed generations(DGs) and coordinate the contradiction between large power grids and DGS[1], microgrids(MGs) have been proposed and received widespread attention. However, due to the access to nonlinear loads, the harmonics are generated [2]. The voltage unbalance and harmonics (the unbalanced voltage and harmonics) will adversely affect equipment and power systems. Also, the stable performance of the system will show [3]. Therefore, the International Electro-technical Commission (IEC) recommends 2% limitation of the voltage unbalance in the electrical system. In addition, the voltage total harmonic distortion (THD) must be less than 5% [4]. Conventionally, through series or active parallel filters (APF), which can select suppressing harmonics, so the voltage unbalanced and harmonics can be compensated. However, the effect is so adverse that it not only increases the total investment cost, but also damages the stability of the grid [5].

Some methods are presented to control the power quality problems. In [6], the synchronous rotating coordinate system, the 5th and 7th harmonics caused by voltage imbalance and harmonic problems are effectively compensated, but there are too many loops and parameters in the control structure, making the reference of the control accuracy insufficient. In [7], the voltage loop of the three-phase four-leg inverter system is introduced, based on the expectation and performance of the transfer function, but the system did not design the current loop control and the dynamic control performance of the current loop was not satisfactory [8–10] According to the microgrid hierarchical control structure, a compensation control strategy for microgrid voltage unbalance and harmonics is proposed, which unfortunately does not consider the issue of DG's ability to compensate the SLB.

✉ Xufeng Liu
624489051@qq.com

[1] Lanzhou Petrochemical Polytechnic, Lanzhou 730060, Gansu, China

[2] Xi'an Technological University, Xi'an 710021, Shanxi, China

[3] Lanzhou University of Technology, Lanzhou 730050, Gansu, China

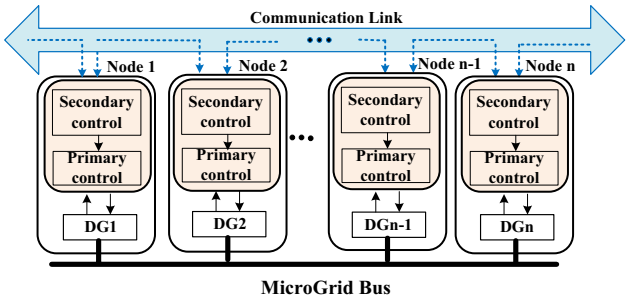

Fig. 1 Networked hierarchical control structure of microgrid

In order to solve all of the problems and accomplish the voltage harmonics compensation simultaneously. In this paper, a hierarchical control scheme (NCS) is proposed to solve the problems of harmonic and voltage unbalance, Fig. 1 shows the networked hierarchical control structure of microgrid, in this structure [11], primary (or named as "local") controller and secondary controller are combined together. They are embedded in each DG, and each DG unit is independently controlled. The local control makes the system variable track its set value with the fastest response speed. The secondary controller collects neighboring unit's data and analyzes the signal, thus every DG's secondary controller can produce appropriate control signal, to realize the voltage unbalance and harmonics compensation at SLB. Meanwhile, all secondary controllers are connected to each other through the network. It makes the microgrid easy to achieve standardization and "plug and play." Although the "plug and play" technology changes structure of MG in order to communicate with network system, a robust algorithm is still needed to enable the system to run stably when communication is blocked in the distributed control system and all nodes need to reach a consensus. When the distributed consensus algorithm is used to solve all the problems, each networked node only needs to communicate with its neighboring node units to obtain a global average value, achieving global information consistency and reducing the communication system burden [12].

The paper is organized as follows. Chapter 2 discusses the networked hierarchical control approach for microgrid. Chapter 3 designs the control system method the approach of the control system, including primary control strategy and DCS strategy. Chapter 4 proposes the method voltage unbalance and harmonic compensation. Section 5 analyzes the stability of the system. Chapter 6 contains simulation and experimental results. Finally, the conclusion is drawn in chapter 7.

2 Networked hierarchical control approach for microgrid

Figure 2 shows the detailed block of networked hierarchical control in each DG unit. In the main circuit, as it is shown in the fig, it consists of a DC power, an LC filter, a three-phase bridge inverter and loads. The loads of the system are different, including balanced/unbalanced loads and linear/nonlinear loads, which are all connected with the system. The local/primary controller has six kinds of modules including voltage loop module, current control loop module, virtual impedance loop module, power droop controller module, power calculation module and positive and negative sequence calculation module. They work together to maintain basic control. The secondary controller contains unbalanced and harmonics compensation module, voltage control module, frequent control module and reactive power control module. It gets the signal from the SLB voltage, then, to calculate Unbalance Factor (UF) and harmonic distortion (HD) indices of the system, and then analyze and process control signals according to requirements. In the main circuit, this paper applies APF to cooperate with DG for compensation. When the voltage unbalance and harmonics are very serious at the SLB, DG is used to compensate for the voltage quality at the SLB, which has exceeded the DG level. Within the

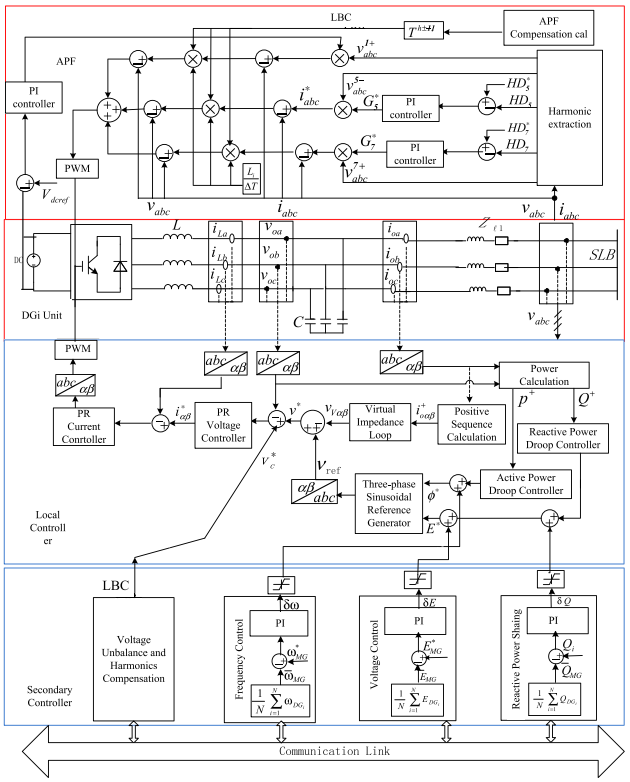

Fig. 2 Diagram of control system

scope of the compensation capability, the APF-coordinated compensator is used to compensate, therefore solving the problem effectively. The other DGs have the same power stage. More details will be introduced in the next chapter.

3 DG primary control

3.1 The modified droop controller

In [13], the theory of instantaneous power is introduced. The active/ reactive power is calculated and is used in the following equations. The fundamental positive sequence active/ reactive power is obtained by a low-pass filter.

$$\omega^* = \omega_0 - (m_P + m_D s)P^+ \tag{1}$$

$$E^* = E_0 - n_q Q^+ \tag{2}$$

In the equations, m_P and m_D are active power proportional and active power integral coefficient; n_q is reactive power proportional coefficient; E_0 is rated voltage amplitude; ω_0 is rated angular frequency. The active power droop controller is used to share the common loads at SLB, and the reactive power control method depends on the MG parameters. However, the frequency/voltage deviations make the system unstable in the secondary controller, combining with the variable deviation value in the secondary controller. In this paper, the droop controller approach is proposed to overcome the problems. As mentioned before, the outputs $\delta\omega$,δE and δQ obtained from secondary control are applied to the droop control, which also changes the droop control curve. The final result is that the voltage and frequency of the system are adjusted, and the reactive power of the system is evenly divided. Equations (1) and (2) are expressed as the following:

$$\omega_i^* = \omega_0 - (m_P + m_D s)P^+ + \delta\omega \tag{3}$$

$$E_i^* = E_0 - n_q Q^+ + \delta E + \delta Q \tag{4}$$

4 The modified virtual impedance loop

The basic structure of virtual impedance appears to be relatively simple [14]. It has no significant effect on the fundamental negative sequence and h harmonic currents and also cannot achieve the decoupling of active and reactive power. The equalization effect of fundamental negative sequence current and harmonic current becomes worse, causing circulation phenomenon inside the system. This paper uses the modified virtual impedance loop, which can be seen in Fig. 3 and the equation is expressed as the following:

$$v_{vr\alpha} = R_{vr}^{1+} i_{o\alpha}^{1+} - L_{vr}\omega_0 i_{o\beta}^{1+} + R_{vr}^{1-} i_{o\alpha}^{1-} \ldots + R_{vr}^{h} i_{o\alpha}^{h} \tag{5}$$

$$v_{vr\beta} = R_{vr}^{1+} i_{o\beta}^{1+} + L_{vr}\omega_0 i_{o\alpha}^{1+} + R_{vr}^{1-} i_{o\beta}^{1-} \ldots + R_{vr}^{h} i_{o\beta}^{h} \tag{6}$$

R_{vr}^{1+},R_{vr}^{1-} and R_{vr}^{h} are virtual resistance for fundamental positive/negative sequence, and h th harmonic components output current.L_{vr} and ω_0 are virtual inductance and angular frequency. $i_{o\alpha}^{1+}$,$i_{o\beta}^{1+}$ is the fundamental positive sequence component of the output current. $i_{o\alpha}^{h}$,$i_{o\beta}^{h}$ is the h th harmonic positive sequence component of the output current.

4.1 The modified quasi Proportional–Resonant(PR) controllers

For the reason that the proportional–integral (PI) controller cannot well realize the steady state tracking control of the sinusoidal signal, this paper uses the PR controller to control the voltage and current loops. This controller can eliminate the control error caused by the PI controller and the large amplitude gain of the ideal resonant controller at the resonance frequency. The most important thing is that the multi-resonance controller can track the multiple harmonic components [15] and [16], so it can be used in the processing of harmonics, and the PR controllers can be expressed as the following:

$$G_V(s) = k_{pV} + \sum_{h=1,3,5,7} \frac{2k_{rV} \cdot \omega_{cV} \cdot s}{s^2 + 2\omega_{cV} \cdot s + (h\omega_0)^2} \tag{7}$$

$$G_I(s) = k_{pI} + \sum_{h=1,3,5,7} \frac{2k_{rI} \cdot \omega_{cI} \cdot s}{s^2 + 2\omega_{cI} \cdot s + (h\omega_0)^2} \tag{8}$$

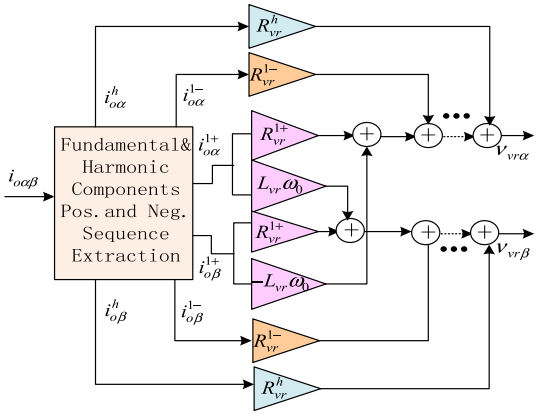

Fig. 3 Virtual impedance

Here, k_{pV} (k_{pI}) and k_{rV} (k_{rI}) are proportional and h th harmonic resonant coefficients of the voltage (current) controller; w_{cV} and w_{cI} are voltage and current controller cutoff frequencies.

5 The secondary controller

5.1 The DSC approach for frequency/voltage restoration and power sharing

In this section, a distributed secondary control is designed to control the frequency and voltage in each DG to the reference [17]. The reactive power of DG is allocated according to the droop coefficients used for primary control of islanded MG. Therefore, the reactive power allocation for secondary control is designed firstly [18].

In the frequent control module, using the consensus algorithm, the average frequency of control system is obtained, and then the average value is sent to other DG units through the communication network. When the obtained average value is compared with the reference value, the frequency deviation value will be obtained by PI controller, finally sending the frequency deviation signal to the primary controller. As seen in Fig. 2, the frequency average and frequency deviation as follows:

$$\overline{\omega}_{MG} = \frac{1}{N}\sum_{i=1}^{N}\omega_{DGi} \tag{9}$$

$$\delta\omega = k_{pf}(\omega^*_{MG} - \overline{\omega}_{MG}) + k_{if}\int(\omega^*_{MG} - \overline{\omega}_{MG})dt \tag{10}$$

k_{pf} and k_{if} are the frequency control parameters of the PI compensator;$\overline{\omega}_{MG}$ is the angular frequency average for all DG units;$\delta\omega$ is the secondary control signal of frequency deviations.

The same method can be used in the voltage control module, and the voltage average and voltage deviation are as follows:

$$\overline{E}_{MG} = \frac{1}{N}\sum_{i=1}^{N}E_{DGi} \tag{11}$$

$$\delta E = k_{pE}(E^*_{MG} - \overline{E}_{MG}) + k_{iE}\int(E^*_{MG} - \overline{E}_{MG})dt \tag{12}$$

k_{pE} and k_{iE} are the voltage control parameters of the PI compensator of unit;E^*_{MG} is the reference voltage and $\overline{E}_{MG}$ is the voltage average for all DG units; δE is the signal of voltage deviation.

In reactive power control module, the reactive power average and reactive power deviation are as follows:

$$\overline{Q}_{MG} = \frac{1}{N}\sum_{i=1}^{N}Q_{DGi} \tag{13}$$

$$\delta Q = k_{pQ}(Q_i - \overline{Q}_{MG}) + k_{iQ}\int(Q_i - \overline{Q}_{MG})dt \tag{14}$$

k_{pQ} and k_{iQ} are the reactive power control parameters of the PI compensator of unit; Q_i is the locally calculated reactive power; $\overline{Q}_{MG}$ is the reactive power average for all DG units; δQ is the signal of reactive power deviation.

Finally, the $\delta\omega$, δE and δQ are obtained from secondary control and change the droop control curve. The equations are shown in (1) and (2).

5.2 The DSC approach for voltage unbalanced harmonic compensation

The secondary controller is designed to compensate voltage unbalance and harmonic, which is shown in Fig. 4. The controller consists of two parts: the block of voltage unbalance factor (UF) & harmonic distortion (HD) indices calculation and the block of compensation effort.

Firstly, a fast selective harmonic extraction method based on cascade delayed signal cancellation (CDSC) is applied to extract the fundamental and harmonics component. The method can flexibly extract selective harmonic sequence from the distorted signals and it also can achieve high detection accuracy and shorter dynamic response time [19]. As seen from Fig. 4, $v^{1+}_{\alpha\beta}$ and $v^{1-}_{\alpha\beta}$ are used to calculate UF and $v^{h+}_{\alpha\beta}$ and $v^{h-}_{\alpha\beta}$ are used to calculate HD^{h+} and HD^{h-}. The calculation equation is expressed as the following:

$$\begin{cases} VUF = \dfrac{V^{1-}_{rms\alpha\beta}}{V^{1+}_{rms\alpha\beta}} \\ HD^{h\pm}_{V} = \dfrac{V^{h\pm}_{rms\alpha\beta}}{V^{1+}_{rms\alpha\beta}} \end{cases} \tag{15}$$

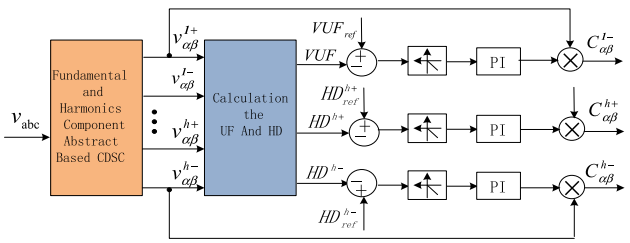

Fig. 4 Compensation of secondary controller

$$\begin{cases} C_{\alpha\beta}^{1-}=\left(VUF_{ref}-VUF\right)\cdot PI(s)\cdot v_{\alpha\beta}^{1-} \\ C_{\alpha\beta}^{h+}=\left(HD_{ref}^{h+}-HD_{V}^{h+}\right)PI(s)\cdot v_{\alpha\beta}^{h+} \\ C_{\alpha\beta}^{h-}=\left(HD_{ref}^{h-}-HD_{V}^{h-}\right)PI(s)\cdot v_{\alpha\beta}^{h-} \end{cases} \tag{16}$$

The UF,HD^{h+} and HD^{h-} are compared with UF_{ref},HD_{ref}^{h+} and HD_{ref}^{h-}, the errors results are sent to the PI controller. Then, the outputs value is multiplied by $v_{\alpha\beta}^{1\pm}$ and $v_{\alpha\beta}^{h\pm}$, finally generating the compensation $C_{\alpha\beta}^{1-}$ and $C_{\alpha\beta}^{h\pm}$.

6 The APF-coordinated compensator

In traditional power systems [20], APF is used to compensate for harmonic currents generated by nonlinear loads. In this paper, we use APF to compensate unbalanced harmonic distortions. It can compensate both the voltage HD and the current HD at SLB. In the island, APF cooperates with DG to complete the voltage compensation in the secondary controller. In the connect grid, the voltage and current are eliminated of the SLB. Finally, the unbalanced harmonic voltage and current are suppressed. Its structure control is shown in Fig. 2. As it can be seen, the APF can detect the voltage and current at the SLB. Through the measurement and extraction module, the harmonic components, fundamental negative sequence components and HD of system are obtained. Then comparing the HD with the HD_{ref}, the conductance value of each order is obtained by PI control. The conductance and the voltage calculate the current reference. According to the literature [21], the equation can be expressed as follows:

$$i_{abc}^{*}=\sum_{h}G_{h}^{*}\cdot v_{abc} \tag{17}$$

where h is the order of the harmonic, G_h^* is the conductance value of each order which the conductance value of the fundamental wave and each harmonic is different;v_{abc} is the voltage value of the fundamental wave and each harmonic at SLB.

The reference of v_{abc}^{*} can be expressed as follows:

$$v_{abc}^{*}=v_{abc}-\frac{L_F}{\triangle T}(i_{abc}^{*}-i_{abc}) \tag{18}$$

L_F is the inductance of APF and $\triangle T$ is the adoption period.

6.1 The voltage compensation of APF

When the DG compensator cannot fully compensate the SLB by itself, the APF controller can calculate compensation through coordinated control management, then using the APF auxiliary compensator for compensation. In the controller, in order to optimize the compensation and make the investment effective, the APF auxiliary compensator avoid being used, and let DG play a major role in the compensation system.

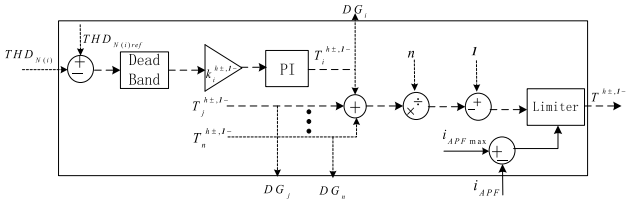

Fig. 5 Calculation of APF coordination compensation

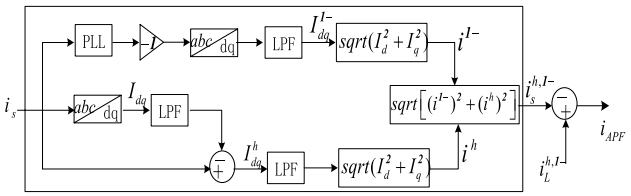

Fig. 6 APF current compensation

In Fig. 5, we can see he $THD_{N(i)}$ is compared with the reference value of THD_{ref}. If the actual value exceeds the reference value of the harmonic, the value $T_i^{h\pm,1-}$ is sent to the DG through low-bandwidth communication (LBC). Finally, the reference voltage is synthesized in local controller, the different DGs produce different parameters $T_j^{h\pm,1-}$ 、$T_h^{h\pm,1-}$ [22]. Finally, the APF coordination compensation is obtained, the equation can be expressed as follows:

$$T^{h\pm,1-}=1-\frac{\sum_{i=1}^{n}T_i^{h\pm,1-}}{n} \tag{19}$$

where $THD_{N(i)}$ is total harmonic distortion rate, $T_i^{h\pm,1-}$ is adjusted by the integral controller, which changes between 0–1; the DG compensation is accompanied by changes between 0–100%. When PCC is fully compensated by DG, $\sum_{i=1}^{n}T_i^{h\pm,1-}=1$.

6.2 The current compensation of APF

In the connect grid, this paper uses APF to compensate the current at SLB. The interference of SLB's voltage and current is reduced in a certain range before and after grid connect to avoid fluctuations in the large power grid. The current compensation of APF is shown in Fig. 6.

The figure shows the DG terminal current. It can be seen that the i^{1-} and the i^{h} are obtained, also the i_{APF} can be obtained from i_L and i_s, the equation can be expressed as follows:

$$i_{APF} = i_L^{h\pm,1-} - i_s^{h\pm,1-} \tag{20}$$

$i_L^{h\pm,1-}$ is the fundamental negative sequence and harmonic current at the load terminal;$i_L^{h\pm,1-}$ is the fundamental negative sequence and harmonic current at the DG terminal.

7 The simulation experimental results analysis

The simulation uses the MATLAB/Simulink software, and the test system are shown in Fig. 7, which consists of two DG inverters forming in MG. A single-phase resistive load is connected at SLB; unbalanced nonlinear load is connected by a 50 Ω linear load and a capacitor. Also, a star-connected linear load (ZL) is connected to SLB. The rated power of DG1 interface inverter is double of DG2 respective value ($S_{01} = 2S_{02}$). The microgrid is rated at 230 V (phase rms voltage) and 50 Hz. Switching frequency of the DGs' inverter is set to 10 kHz.

In the paper, the parameters remain consistent with [23]. Tables 1 and 2 show the parameters of electrical systems and control system. Table 3 is the secondary PI control parameters. In Fig. 7, Z_{l1} and Z_{l2} are the impedance between DGs and SLB. The compensation time starts at t = 0.5 s. UF* is set to 0.5%; THD* is set to 2.5%.

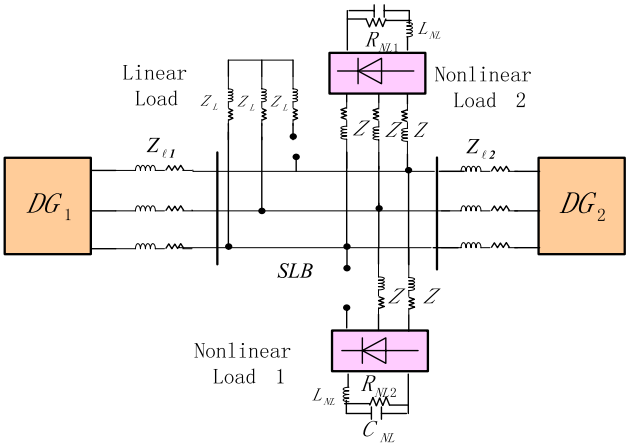

Fig. 7 Test system of simulation studies

Table 2 Control system parameters

Power controllers (DG1/DG2)					
m_D (rad/W)		m_D (ras/W. s)		$n_q(V/VAr)$	
$0.6\times10^{-5}/1.2\times10^{-5}$		$0.6\times10^{-4}/1.2\times10^{-4}$		$1.4\times10^{-1}/2.8\times10^{-1}$	
Virtual impedance (DG1/DG2)					
R_{vr}^{1+} (Ω)	L_{vr}(mH)	R_{vr}^{1-} (Ω)	R_{vr}^{3} (Ω)	R_{vr}^{5} (Ω)	R_{vr}^{7} (Ω)
0.3/0.6	2.5/5	1.5/3	2/4	4/8	4/8
Voltage/Current controller					
K_{pV}/K_{p1}	K_{rV1}/K_{rI1}	K_{rV3}/K_{rI3}	K_{rV5}/K_{rI5}	K_{rV7}/K_{rI7}	ω_{cV}/ω_{cI}(rad/s)
1/5	100/1000	200/400	50/100	100/100	2/2

Considering the compensation control to the voltage unbalance and the harmonic, the UF and HD of DGs and SLB are shown in Fig. 8. In Fig. 8a, UF of SLB can properly follow the reference value after compensation control. Also, due to the compensation given by the DGs voltage, the voltage quality of SLB has been improved. In Fig. 8a, also, because the line impedance of DG1 is slightly larger than DG2, the UF of DG1 increases more than DG2. From Fig. 8b, the SLB voltage quality is distorted noticeably before 0.5 s and the voltage HD of SLB is higher before 0.5 s. But after the proposed compensation control, the HD also gets improved greatly; the voltage harmonic distortion index HD at 3rd, 5th and 7th voltage frequency is also below 5%. In Fig. 8, the comparison of simulation results proves that the proposed compensation approach has better effect.

In order to eliminate the influence caused by the deviation of the voltage and frequency, the DSC approach for frequency/voltage is introduced in Sect. 4. The output voltage and frequency of the local controller are affected by active and reactive power and the voltage amplitude and frequency haven't reached the reference values. According to the consensus algorithm of DSC, the voltage and frequency are obtained in Eq. (17), the deviation of DG voltage amplitude is eliminated within 0.5 s, and the final voltage amplitude reaches the required voltage reference value. The frequency deviation elimination method of DG is the same as voltage

Table 1 Main circuit parameters

APF		LC Filter Inductance	LC Filter capacitance	Nonlinear loads Tie lines
$L_{F(\mathrm{mH})}$	$C_F(\mu F)$	L (mH)	C (μF)	$Z(\Omega, mH)$
15	2200	2	25	0.12, 1.8
Distribution Lines		Nonlinear loads		Linear loads
Z_{l1}, Z_{l2} (Ω, mH)		C_{NL}/R_{NL1}, R_{NL1}/L_{NL} $(\mu F/\Omega/mH)$		Z_L (Ω, mH)
0.1, 1.6		235, 50, 200/0.080		50,20

Table 3 PI control parameters of DSC

Fundamental negative sequence		3rd Harmonic positive and negative sequences	
Proportional	Integral	Proportional	Integral
3	90	1.25	110
5th Harmonic positive and negative sequences		7th Harmonic positive and negative sequences	
Proportional	Integral	Proportional	Integral
1	150	0.95	200

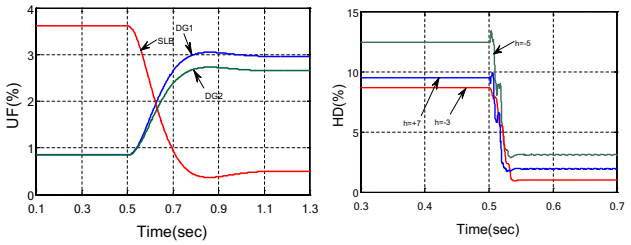

(a) The UF of voltage **(b)** The HD at 3rd, 5th and 7th of voltage

Fig. 8 Before and after compensation

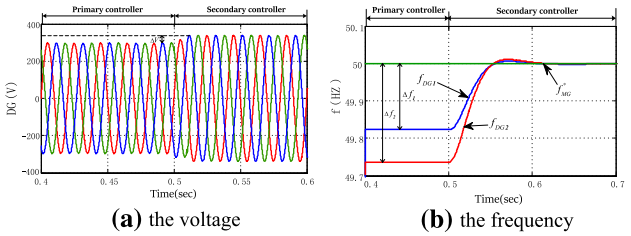

(a) the voltage **(b)** the frequency

Fig. 9 Output waveform of secondary control

deviation. The frequency deviation is eliminated so that the frequency reaches its reference value. In Fig. 9, the voltage and frequency are adjusted through secondary controller. It can be clearly seen that the deviation of voltage amplitude and frequency has been eliminated, thus it is necessary to increase secondary control.

Figure 10 shows the output power of DGs. In Fig. 10a, according to system's capacity, the system's active power is distributed 1:1 before 0.5 s compensation, and secondary control is added in 0.5 s. Obviously, the active power increases and is still divided equally. In Fig. 10b, according to the system capacity setting, the reactive power of DG is distributed 2:1 before 0.5 s compensation. The secondary control was added after 0.5 s. due to the calculation of the distributed consensus algorithm, the reactive power is evenly divided after compensation (the same voltage and frequency). Namely, the reactive power of the two DGs is equally distributed.

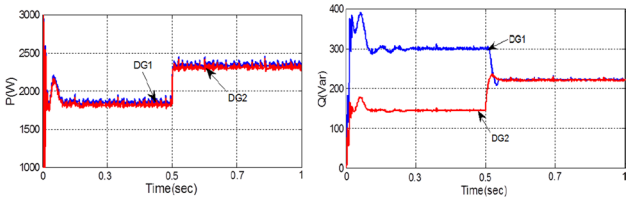

(a) the active power **(b)** the reactive power

Fig. 10 Waveforms before and after compensation

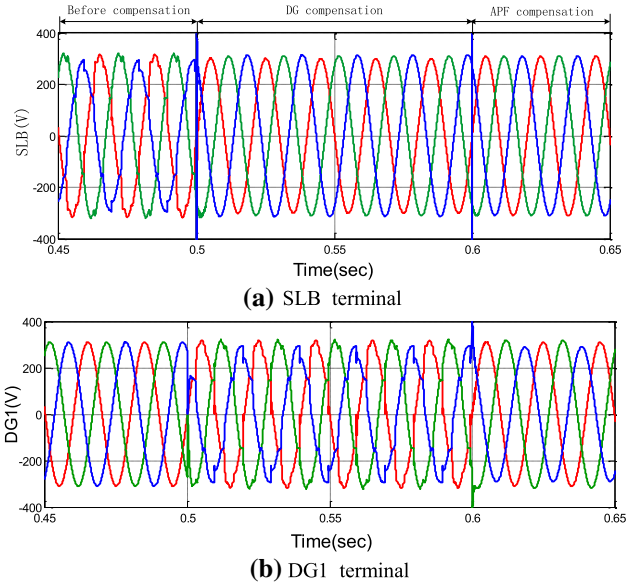

(a) SLB terminal **(b)** DG1 terminal

Fig. 11 Before and after voltage compensation

We can see the compensation of unbalanced harmonic at DG1, DG2, and SLB in fig. Add the DG's own compensation to 0.5 s and add the APF's coordinated compensation to 0.6 s. In Fig. 11a, with the connection of the unbalanced nonlinear load, the voltage quality is poor of the SLB. When the DG compensator is connected in 0.5 s, with the self-compensation of DG, the voltage quality has been significantly improved at SLB. However, the DG's own compensation ability is limited, and the voltage quality of SLB still has a slight voltage distortion and unbalance. Then, the

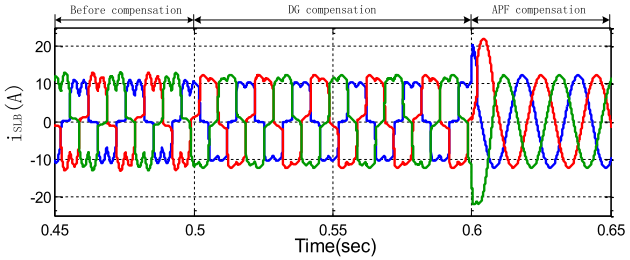

Fig. 12 Before and after current compensation

APF-coordinated compensator is connected in 0.6 s and the voltage quality of SLB was completely compensated. This compensation effect is obvious. Also, in Fig. 11b, the voltage quality of the DG1 terminal before compensation is very good. Nevertheless, because DG compensates the voltage quality of SLB in 0.5 s, its own voltage becomes distorted and unbalanced. In 0.6 s, due to the voltage compensation of SLB by the APF-coordinated compensator, the voltage distortion at DG terminal is also compensated incidentally. The analysis of DG2 is same with DG1.

The analysis of current is the same as voltage. Figure 12 shows the waveform of current at SLB, due to the connection of the unbalanced nonlinear load, the current is severely distorted and unbalanced before compensation. The DG's own compensator is added to 0.5 s. Because the DG compensation is voltage compensation, the current waveform has a slight change. When the APF-coordinated compensator is added to 0.6 s, the APF can compensate the current that is completely compensated. This compensation effect is obvious.

Compared with the traditional method, the traditional compensation method is to compensate the power quality of the SLB through the control of DG itself. This paper proposes to add APF to cooperate with DG to complete the control compensation. When the power quality at the SLB is poor and exceeds the compensation range of the DG, it is switched to APF to supplement. When it can compensate within its own range, DG completes its own compensation. This not only improves equipment utilization, but also better understand equipment performance.

8 Conclusion

This paper conducts a research on the unbalance and harmonic problems in the microgrid, based on the structure of hierarchical control and combined with APF. Meanwhile, a networked hierarchical control approach is proposed. In the control approach, the microgrid system consists of primary and secondary control. For the primary controller, the structure and performance are mainly concerned, which are important in the stable operation of microgrid. In the secondary controller, the power quality is controlled in the voltage unbalance and harmonic compensation module; then, the voltage amplitude, frequency and reactive power deviation are optimized by using the distributed consistency algorithm of the microgrid. The DG compensation and APF-coordinated compensation controller are designed, which coordinate with each other to control the power quality of the system. Finally, simulation and experiment waveforms can prove the effectiveness of the proposed control method.

Funding Gansu Province Innovation Ability Improvement Project (No.2019B-235). Lanzhou science and technology development guiding plan project (No.2019-zd-160).

References

1. Afshari E, Moradi GR, Rahimi R (2017) Control strategy for three-phase grid-connected PV inverters enabling current limitation under unbalanced faults. IEEE Trans Industr Electron 64(11):8908–8918
2. Cañizares CA, Palma-Behnke R (2014) Trends in microgrid control. IEEE Trans Smart Grid 5(4):1905–1918
3. Papič I, Matvoz D (2019) A benchmark test system to evaluate methods of harmonic contribution determination. IEEE Trans Power Delivery 34(1):23–31
4. IEEE Standard for Interconnecting Distributed Resources With Electric Power Systems, IEEE 1547–2003, 2003.
5. Micallef A (2014) Maurice Apap, "reactive power sharing and voltage harmonic distortion compensation of droop controlled single phase islanded microgrids." IEEE Trans Smart Grid 5(3):1149–1158
6. Yao J, Zhu W (2019) Unbalanced harmonic suppression of three-level active power filter with optimal hybrid control. In: 2019 IEEE 10th International Symposium on Power Electronics for Distributed Generation Systems (PEDG), pp 207–211
7. Hamzeh M, Karimi H, Mokhtari H (2014) Harmonic and negative-sequence current control in an islanded multi-bus mv microgrid. Trans Smart Grid 5(1):167–176
8. Pola G, Pepe P, Di Benedetto MD (2018) Decentralized supervisory control of networks of nonlinear control systems. IEEE Trans Autom Control 63(9):1349–1361
9. Wu L, Yang X, Hao X, Lei Y (2015) Networked hierarchical control scheme for voltage unbalance compensation in an islanded microgrid with multiple inverters. IEEE Int J Innov Comput Inf Control 45(2):1349–1361
10. Liang Z, Guo Y, Yang Y, Chen G (2019) Distribution network control system scheduling strategy. In: 2019 IEEE 3rd Information Technology, Networking, Electronic and Automation Control Conference (ITNEC), pp 1424–1428
11. Lai J, Lu X, Yu X, Yao W, Wen J, Cheng S (2019) Distributed multi-DER cooperative control for master-slave-organized microgrid networks with limited communication bandwidth. IEEE Trans Ind Informat 15(6):3443–3456
12. Wu L, Hao X (2016) Decentralized control approach for voltage unbalance compensation in islanded microgrid. In: 2016 IEEE 8th International Power Electronics and Motion Control Conference (IPEMC-ECCE Asia), pp 1349–1361
13. Chatterjee D, Dalapati S (2020) Single-phase average power measurement using instantaneous power theory in a fixed point

processor. In: 2020 IEEE Calcutta Conference (CALCON), pp 297–301
14. Savaghebi M, Jalilian A, Vasquez JC, Guerrero JM (2013) Autonomous voltage unbalance compensation in an islanded droop-controlled microgrid. IEEE Trans Ind Electron 60(4):1390–1402
15. Hans F, Schumacher W, Chou S-F, Wang X (2020) Design of multifrequency proportional-resonant current controllers for voltage-source converters. IEEE Trans Power Electron 35(12):13573–13589
16. Geeta, M. S. Aspalli (2020) Proportional resonant controller for semi converter three phase VSI fed induction motor drive to enhance time response. In: 2020 International Conference on Power Electronics & IoT Applications in Renewable Energy and its Control (PARC), pp 994–1004
17. Hou X, Sun Y, Liu Z, Han H, Su M (2016) Stability analysis and stabilization methods of DC microgrid with multiple parallel-connected DC–DC converters loaded by CPLs. IEEE Trans Smart Grid 9(1):132–142
18. Mahmoud MS, AL-Sunni FM (2015) Control and Optimization of Distributed Generation Systems. Springer Science and Business Media LLC, 58(1), 127–138
19. Savaghebi M (2012) Student Member, Secondary Control for Voltage Quality Enhancementin Microgrids. IEEE Trans Smart Grid. 3(4):3984–3995
20. Yan Y, Sun N, Zhang N (2020) Hierarchical reliability evaluation to security and stability control system of power systems. In: 2020 5th Asia Conference on Power and Electrical Engineering (ACPEE), pp 4488–4497
21. Lee TL, Cheng PT (2017) Design of a new cooperative harmonic filtering strategy for distributed generation interface converters in an islanding network. IEEE Trans Power Electron 22(5):1919–1927
22. Mousavi SYM, Jalilian A, Savaghebi M (2018) Autonomous control of current- and voltage-controlled DG interface inverters for reactive power sharing and harmonics compensation in Islanded Microgrids. IEEE Trans Power Electron 33(11):9375–9386
23. Yang Z, Sun J, Li S, Huang M, Zha X, TangAn Y (2018) Adaptive carrier frequency optimization method for harmonic energy unbalance minimization in a cascaded H-bridge-based active power filter. IEEE Trans Power Electron, pp 1024–1037